Progress In Electromagnetics Research B, Vol. 57, 115–126, 2014

A Preprocessing Filter for Multistatic Microwave Breast Imaging for Enhanced Tumour Detection

Atif Shahzad, Martin O'Halloran*, Edward Jones, and Martin Glavin

Abstract—Ultra Wideband Radar imaging has shown promising results in the detection of small tumours within low to medium density human breasts. A wide range of beamforming algorithms has been presented in several recent studies with good tumour localization capabilities, but most of these suffer a deterioration in performance with an increase in breast tissue density. In this paper, a preprocessing filter is used to compensate for path-dependent attenuation and phase effects, in conjunction with a range of existing data-dependent and data-independent confocal microwave imaging algorithms. Results indicate that this data preprocessing improves the performance of all beamformers, enabling detection and accurate localization of multiple tumours in mild to moderately dense human breasts. The proposed framework is tested on 3D anatomically accurate numerical breast models and the performance is evaluated across a range of appropriate metrics.

1. INTRODUCTION

Breast cancer represents 31% of all cancers in women, with an approximate 1.38 million sufferers worldwide. The estimated death toll due to breast cancer in 2011 was 39,520 in the U.S. [1] and 11,650 in UK [2]. The current standard breast screening modality is X-Ray mammography. Although it has shown good cancer detection capabilities, mammography has a number of well-known limitations, particularly in dense breast tissue [3]. Studies have shown that a tumour occurring in dense glandular breast is often likely to be missed by X-Ray mammography [4]. This limitation of X-Ray mammography, coupled with other adverse physiological effects, motivate the development of alternate breast imaging modalities with enhanced sensitivity and specificity.

Several prototype microwave breast imaging systems have been developed in recent years, and almost all of them are based on studies that confirm existence of significant dielectric contrast between different types of breast tissues at microwave frequencies. Early studies reported that the dielectric contrast between normal and malignant tissues was sufficiently high to differentiate between them [5, 6]. Historically, researchers sought to exploit this contrast and developed microwave imaging techniques to localize and classify malignant tissues in human breast. Two major microwave imaging approaches were examined: Microwave Tomography [7] and Ultra-Wideband (UWB) Radar Imaging [8]. This paper specifically addresses UWB Radar Imaging.

UWB Radar Imaging uses the back-scattered electromagnetic energy from microwave scatterers within the breast to create an image. Hagness et al. [9] developed one of the first beamforming algorithm based on the Confocal Microwave Imaging (CMI) approach. Since then, there has been a large amount of research on the refinement of radar based beamformers [10, 11]. However, each of these algorithms is based on several assumptions regarding the relative dielectric properties of normal and cancerous breast tissue. One of the most important assumptions is that the breast is primarily dielectrically homogeneous; and consequently that the dielectric properties of normal tissue allow for coherent addition of the UWB backscattered signals.

Received 6 August 2013, Accepted 18 November 2013, Scheduled 1 December 2013
* Corresponding author: Martin O'Halloran (martin.ohalloran@gmail.com).
The authors are with the Electrical and Electronics Engineering, National University of Ireland Galway, Galway, Ireland.

However, a recent study of the dielectric properties of breast tissue has highlighted the dielectric heterogeneity of normal breast tissue [12]. Lazebnik et al. found a very significant dielectric contrast between healthy adipose and glandular tissue within the breast. This heterogeneity of normal breast tissue had not been considered in previous beamformer designs and the difficulty this presents to traditional beamformers was highlighted in a recent study by O'Halloran et al. [13]. The relatively small dielectric contrast between fibroglandular and cancerous tissues often makes it difficult to detect a tumour within dense glandular human breast. The presence of glandular tissue with higher dielectric properties introduces a significant amount of attenuation and dispersion in the signal, and in these circumstances conventional beamforming algorithms often fail to detect and localize the tumour. An effective means for reducing the effects of dispersion due to heterogenous tissue will enable a beamformer to better differentiate between adjacent dielectric scatterers within the breast, providing a much improved image of any tumours present.

In this paper, a preprocessing approach to compensate for attenuation and dispersion effects is described and the resultant signals are processed by a range of data-dependent (DD) and data-independent (DI) beamformers. Test data are generated using anatomically accurate electromagnetic breast models, based on Lazebnik's study. The pre-filtering approach is a novel technique that can be used to enhance the image quality of existing beamformer. It was previously described by the authors and used in conjunction with mono-static Delay And Sum (DAS) beamformer algorithm [14]. In this study, the application of the proposed preprocessing filter has been extended from monostatic to multistatic and applied to a range of beamformers. The efficacy of the proposed filter as general preprocessing approach on multistatic signals is evaluated. It is shown that the proposed filter can be used to improve upon the performance of a number of existing multistatic DI and DD beamforming algorithms. In particular, the performance of the preprocessing filter, in conjunction with the conventional Delay And Sum (DAS) beamformer, Improved Delay And Sum (IDAS) beamformer, Delay Multiply And Sum (DMAS) beamformer, Robust Capon Beamformer (RCB), and Multistatic Adaptive Microwave Imaging (MAMI), is examined and evaluated with respect to several performance metrics. The remainder of the paper is organized as follows: Section 2 describes the preprocessing filter design; Section 3 details the numerical breast models and simulation setup used to evaluate the method; Section 4 describes the DD and DI beamformers; Section 5 presents the performance metrics and results; finally, conclusions are detailed in Section 6.

2. DESIGN OF PRE-PROCESSING FILTER

In the pre-filtering approach described here, the recorded multistatic radar signals are filtered to compensate for dispersion and attenuation before applying any beamforming algorithm. Assuming that the average dielectric parameters of the breast can be estimated *a-priori*, a compensation filter to remove a significant portion of the dispersion and attenuation effects introduced by the breast can be designed. The filter design process will be described in more detail in the following section.

2.1. Artifact Removal

Prior to application of pre-filtering, it is assumed that artifacts such as skin reflections, antenna coupling and reverberation effects have been removed. The artifact due to mutual antenna coupling and reverberation effects are removed by subtracting measurements from the system recorded in the absence of a breast phantom. A range of existing artifact removal algorithms such as given in [15] can be used to remove the air-skin artifact before filtering. The primary focus of this paper is preprocessing for improved breast cancer detection; therefore, in this study these artifacts are removed using an ideal artifact removal method as used by Bond et al. [16].

2.2. Compensation Filter Design

In order to design the filter, the average dielectric properties of the breast under examination must be established. Since the average dielectric properties of the breast will vary significantly between patients, this study assumes that these properties have been established *a-priori* using an appropriate patient-specific estimation algorithm, such as [17–19]. Based on these properties, a Finite Difference Time

Domain (FDTD) breast model is created. The breast is illuminated by a UWB pulse and the reflected signals are recorded. Next, a second set of electromagnetic signals is recorded on an equivalent non-dispersive FDTD model of breast with similar average dielectric properties. These two sets of signals are used to design the compensation FIR filter.

Let $s_i(r,n)$ be the response received at the ith antenna focusing at spatial location r in a 3D dispersive model, $z_i(r,n)$ is the signal received from an equivalent non dispersive model, L is the filter length and N is the length of the sampled signal. Then the least squares solution to the real valued filter design problem, for each antenna location i, is given by:

$$w = R^{-1}p \tag{1}$$

where, $w = [w_0, w_1, \ldots, w_{L-1}]^T$ is a vector of filter coefficient values to be estimated, R is the $L \times L$ autocorrelation matrix of the received dispersive signal $s_i(r,n)$, and p is the $L \times 1$ cross-correlation vector defined as:

$$p = Qz^T \tag{2}$$

The covariance matrix Q is constructed from the received signal as:

$$Q = \begin{bmatrix} s_i(r,L) & s_i(r,L+1) & \cdots & s_i(r,N) \\ \vdots & \ddots & & \vdots \\ s_i(r,1) & s_i(r,2) & \cdots & s_i(r,N-M+1) \end{bmatrix} \tag{3}$$

and the vector z is given as:

$$z = [z_i(r,L), z_i(r,L+1), \ldots, z_i(r,N)] \tag{4}$$

The signals used for the filter design are recorded on each discrete spatial position r over the numerical phantom with estimated average dielectric properties. The distance $d_i(r) = |r - r_i|$, for each focal point in a 3D grid is rounded to the nearest integer value and a vector of unique distance values is created as $d = [d_{\min}, \ldots, d_{\max}]$. The FIR filter weights for the complete set of synthetic focal points in the imaging grid are precomputed. This set of FIR filters is then applied to remove the attenuation and dispersion in the received signals after focusing at each spatial position in the imaging grid. The focus is achieved by time shifting all the signals to align for the focal point r in the grid.

3. NUMERICAL MODELS

The FDTD model must incorporate the heterogeneity and the spatial distribution of different tissues within the breast. The 3D models used in this study are based on the UWCEM MRI-derived Breast Phantom Repository [20]. Two concentric rings of 20 antennas (point source) are positioned around the breast, as shown in Figure 1. The antennas are immersed in a liquid matching the average dielectric properties of adipose as given in Table 1. The dielectric properties of skin, adipose, and fibro-glandular tissue used in the FDTD models are based on Lazebnik's studies [21], and incorporated using Debye models, with the parameters being derived empirically. The Debye parameters for each tissue type, along with the permittivity and conductivity at the center frequency, are given in Table 1.

Three specific scenarios are considered (Figure 2) where (2B) and (2C) are derived from MRI:

- A tumour is homogeneous breast phantom;
- A tumour in a heterogeneous fat-only breast model, with variations in dielectric properties to produce 25 different samples.
- A tumour in a heterogeneous breast with fat and fibro-glandular tissue but positioned in a region of adipose tissue.

A differentiated Gaussian pulse, with a center frequency of 6 GHz and a -3 dB bandwidth of 6.4 GHz is used to illuminate the breast. Prior to any signal processing, all radar signals are down sampled from 599 GHz to 59.9 GHz. A 3D image of the entire breast is created, where the grid dimensions are $190 \times 190 \times 190$ voxels, with resolution of 1 mm^3.

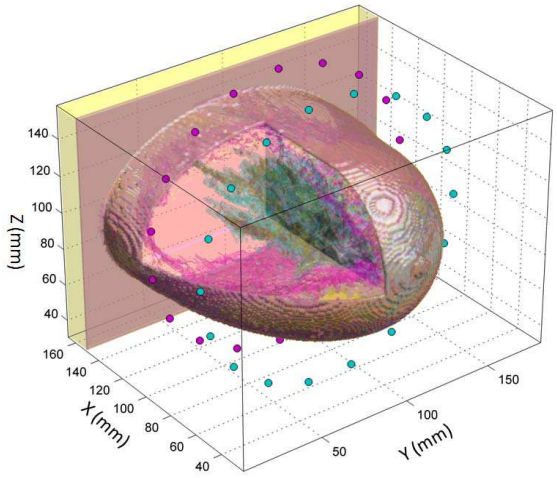

Figure 1. MRI-derived FDTD model and antennas setup.

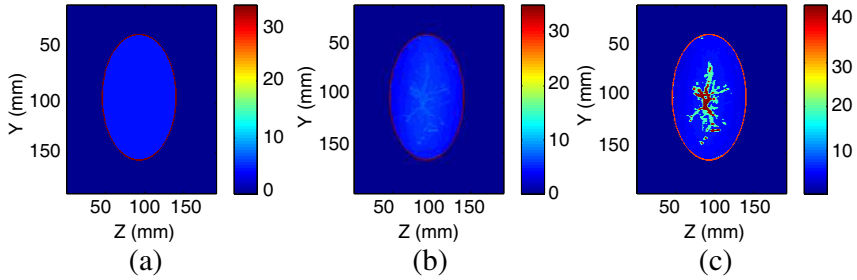

Figure 2. MRI-derived FDTD models.

Table 1. Debye parameters of constituent tissues of the breast used in the FDTD model, and their corresponding relative permittivity and effective conductivity at the center frequency.

Tissue	ε_∞	$\Delta\varepsilon$	σ_s (S/m)	τ (ps)	ε_r	σ_e
Adipose Lowest	2.848	1.104	0.05	13.00	3.738	0.196
Adipose Highest	3.987	3.545	0.180	13.00	6.848	0.657
Fibro-glandular Lowest	11.98	23.55	0.538	13.00	30.94	3.644
Fibro-glandular Highest	14.91	38.55	0.738	13.00	45.99	5.823
Skin	15.93	21.83	0.831	13.00	33.51	3.705
Tumor	20.28	45.05	1.300	13.00	56.60	7.242

4. BEAMFORMERS

Beamforming algorithms perform spatial filtering on data acquired in a radar based system. It is used to focus on a certain spatial position and create a 2D/3D map of reflected energy from an imaging space. Beamforming algorithms are classified into two categories: data-independent (DI) and data-dependent (DD) beamformers. These categories and representative algorithms in each category are explained in following section.

4.1. Data-independent Methods

The DI beamformers use an assumed propagation model to establish the delay and attenuation effects encountered by a radar signal propagating in that channel. The signals are shifted and scaled for a particular focal point in the imaging space. The standard Delay And Sum (DAS) beamformer and two variants used in this study, are explained in the following sub-sections.

4.1.1. Delay and Sum

The DAS beamformer involves the summation of the time-shifted scattered signals from the breast to create a synthetic focus. Consider the case of M multistatic channels and let $s_i(r,n)$ denote the ith scattered discrete time signal from focal point r, then the energy associated with the focal point $r=[x,y,z]$ within the breast is defined as:

$$I(r)=\sum_{n=1}^{T_{win}}\sum_{i=1}^{M} w_n s_i(r,n-\Delta_i(r)) \tag{5}$$

where n is sample index with discrete time delay in the ith channel described as $\Delta_i(r)=(d_i(r))/(vT_s)$, where $d_i(r)=|r-r_i^t|+|r-r_i^r|$ describes the ith channel path length; r_i^t and r_i^r are transmitting and receiving antenna locations; v is the average velocity of signal propagation in breast tissue, T_{win} the window length in time samples, and T_s the sampling interval. The term w_n is a wighting factor to compensate for the attenuation in the signal due to propagation in the lossy medium.

4.1.2. Improved Delay and Sum

Klemm et al. [22] proposed an extended version of DAS, with an additional weighting factor called the Quality Factor (QF). The energy from all the channels at a particular focal point is cumulatively summed and a second order polynomial is fitted to the cumulative energy curve as function of increasing number of channels. The coefficient a of highest order term in the fitted polynomial ($y=ax^2+bx+c$) is considered as the QF.

4.1.3. Delay Multiply and Sum

The DMAS beamformer is another extension of the conventional DAS beamformer, proposed by Lim et al. [23]. It involves paired multiplication of radar signals before summation as an extra measure of coherence.

4.2. Data-dependent Methods

Data-dependent (DD) algorithms adaptively select weight vectors to incorporate the directivity in the beamforming algorithm. Enhanced sensitivity to certain Directions of Arrival (DOA) in the focusing algorithm provides better resolution, and suppression of interference from other scatterers in the imaging space. Two of the major existing beamforming algorithms are used in this study to verify the efficacy of the pre-processing technique with DD beamforming algorithms. These DD beamformers are explained in the following section.

4.2.1. Robust Capon Beamformer (RCB)

A multistatic Robust Capon (RCB) Beamforming algorithm was presented by Xie et al. [24]. The RCB algorithm is described as:

$$\min_{w} \left\{w^T R w\right\} \text{ subject to } w^T a_0 = 1 \tag{6}$$

where $w=[w_1,w_2,\ldots,w_M]^T$ is the weight vector for M multistatic channels, a_0 the steering vector corresponding to the signal of interest, and R the sample covariance matrix. The solution to (6) is

derived as:

$$w = \frac{R^{-1}a_0}{a_0^T R^{-1} a_0} \tag{7}$$

The steering vector a_0 is obtained from:

$$\min_a \left\{ a_0^T R a_0 \right\} \text{ subject to } \|a_0 - \bar{a}\|^2 \leq \epsilon \tag{8}$$

where $\bar{a} = [1, \ldots, 1]^T$ is an assumed steering vector, and factor ϵ is used to describe the uncertainty of a_0. The energy at a given point $r = [x, y, z]$ can be calculated as:

$$I(r) = \sum_{n=1}^{T_{win}} \sum_{i=1}^{M} w_i . s_i(r, n - \Delta_i(r)) \tag{9}$$

4.2.2. Multistatic Adaptive Microwave Imaging (MAMI)

The MAMI algorithm implements a cascaded two-stage RCB to enhance the performance of a single-stage RCB-based beamformer. The estimated signals from stage one can be represented as:

$$\hat{S}(n) = a_s s(n) + e_s(n), \quad n = 1, \ldots, N \tag{10}$$

where $\hat{S}(n), n = 1, \ldots, N$ is a temporal representation of the estimated signals from stage one, a_s denotes the steering vector for second stage, $e_s(n)$ is the estimation error, and $s_n(n)$ is the desired signal that is estimated by:

$$\max_{\sigma^2, a_s} \sigma^2 \text{ subjct to } R_s - \sigma^2 a_s a_s^T \geq 0, \ \|a_s - \bar{a}\|^2 \leq \epsilon_s \tag{11}$$

where $\sigma^2 = 1/N \sum_{n=1}^{N} s^2(n)$ is the power of the signal of interest, ϵ_s the uncertainty parameter in second stage, and R_s the sample covariance matrix given as:

$$R_s = \frac{1}{N} \sum_{n=1}^{N} \hat{S}(n) \hat{S}^T(n) \tag{12}$$

Thus weight vector w_s for the second stage of MAMI can defined as:

$$w_s = \frac{R_s^{-1} a_s}{a_s^T R_s^{-1} a_s} \tag{13}$$

Finally, the energy at focal point $r = [x, y, z]$ in imaging space can be calculated as:

$$I(r) = \sum_{n=1}^{T_{win}} \sum_{i=1}^{M} w_{s_i} \cdot \hat{s}_i(r, n) \tag{14}$$

where $\hat{s}_i(r, n)$ is an estimate of signal $s_i(n)$ in Equation (10) for energy calculation at location r.

5. PERFORMANCE METRICS AND RESULTS

5.1. Metrics

5.1.1. Signal to Mean Ratio

The Signal to Mean Ratio (SMR) describes the ratio of the tumour response to the mean of response of all tissue types within the resultant energy profile. The SMR is given as:

$$\text{SMR} = E_{T_\mu} / E_\mu \tag{15}$$

where E_{T_μ} is the average energy computed over the tumour region (defined by the Full Width Half Maximum (FWHM) metric below) and E_μ is the average energy over whole imaging grid.

5.1.2. Full Width Half Maximum

The physical extent of the tumour is measured by the Full Width Half Maximum (FWHM) metric, and is defined as the distance from the tumour response to where the tumour backscattered energy drops by one half. It is computed over a 2D cross-section of the constructed 3D energy map at the center of the tumour location in each direction, and is averaged over all three directions.

5.1.3. Signal to Clutter Ratio

The Signal to Clutter Ratio (SCR) describes the ratio of maximum energy in the tumour region to maximum energy outside the area defined by the FWHM of the tumour. The SCR is defined as:

$$\text{SCR} = E_{T_{\max}}/E_{C_{\max}} \tag{16}$$

where $E_{T_{\max}}$ is the maximum energy in the tumour region and $E_{C_{\max}}$ is the maximum energy outside the FWHM of tumour response.

5.2. Results

This section describes the effect of the pre-filtering process on the raw radar signals, before illustrating the benefit of the signal pre-processing to all breast beamforming algorithms. Firstly, to clearly show the effects of pre-filtering, a sample received signal ($S_{(1,6)}$ — solid blue, transmitted from antenna 1 and received at antenna 6) is shown in Figure 3, with the corresponding filtered signal shown in red. The inset image in Figure 3 shows a snapshot of the tumour response in the signal. Importantly, the FWHM of the filtered signal is approximately equal to that of the original transmitted pulse, indicating the compensation for path-dependent signal dispersion. This compensation should result in an improved image of the breast.

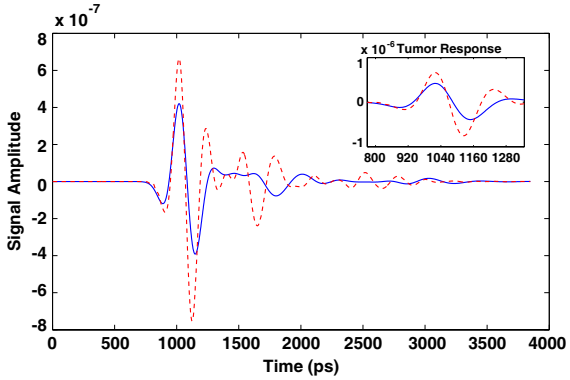

Figure 3. A sample received signal ($S_{(1,6)}$ (solid blue), transmitted from antenna 1 and received at antenna 6) with the corresponding filtered signal shown in red. The pre-filtering process compensates for path-dependent dispersion effects. The scaled tumour response is also shown inset.

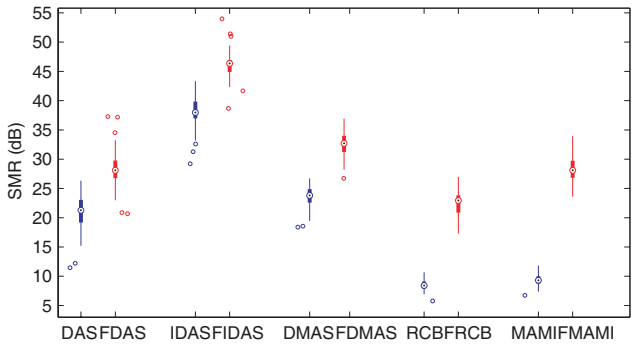

Figure 4. Signal to Mean Ratio: box plot over 25 samples for non-filtered (blue) and pre-filtered (red) beamformers.

Next, imaging results with and without filtering for a range of beamforming algorithms will be presented. Three performance metrics were used as described above to evaluate imaging performance. The detection and localization capabilities are verified by adding accurately modeled malignant tumours of 5 mm, 7 mm and 10 mm in these FDTD breast models. A set of homogeneous (Figure 2(a)) and adipose-only heterogeneous (Figure 2(b)) models with variations in dielectric properties and tumour location were considered, resulting in 25 different clinical scenarios. The box plots of performance metrics for the reconstructed images (with and without pre-filtering) are provided for comparison in Figures 4, 5, and 6.

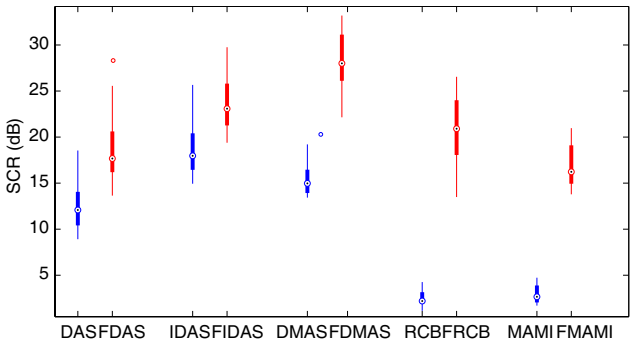

Figure 5. Signal to Clutter Ratio: box plot over 25 samples for non-filtered (blue) and pre-filtered (red) beamformers.

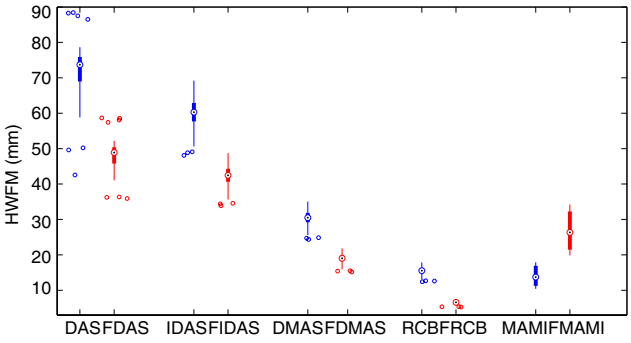

Figure 6. Half Width Full Maximum: box plot over 25 samples for non-filtered (blue) and pre-filtered (red) beamformers.

The pre-filtering approach shows an improvement across all of the five beamformers with an average 11 dB increase in SMR, 10 dB increase in SCR, and 25% reduction in FWHM for detected tumours in the reconstructed images. The reconstructed images (2-D slices) without and with pre-filtering for the DAS, IDAS, DMAS, RCB, and MAMI beamformers (top to bottom respectively) are shown in Figure 9.

The column on the left presents images formed without pre-filtering and the column on the right shows the images with pre-filtering. Clearly pre-filtering provides better clutter-suppression and tumour localisation compared to non-filtered images, especially in the case of DMAS and RCB beamformers. However, it could be argued that all of the five beamformers considered in this study could fail to detect a tumour in a breast with a higher proportion of dense fibro-glandular tissue. This is tested with a dense numerical example (Figure 2(c)) and resulting images are shown in Figure 7. Here the DMAS beamformer is used to reconstruct a 2D slice of a dense dielectrically-heterogeneous breast (the permittivity of the fibro-glandular and tumour tissue in the model are 45 and 56, respectively at the centre frequency of the transmitted pulse). In the original image, the tumour is completely obscured by clutter due to the large region of glandular tissue at the centre of the breast. However, using pre-filtering, the tumour finally becomes discernible, even in this most challenging of breast imaging scenarios.

It is observed that pre-filtering can improve the effective resolution of the signal and imaging results by compensating for dispersion. However, it may introduce a significant amount of noise in the signals if the estimation error in the average dielectric values is higher than 20%. Figure 8 shows plot of Mean Squared Error (MSE) across all the channels in three different scenarios. A filter designed using average estimated values has been applied to three MRI derived numerical phantoms where the estimation error of dielectric properties is 10% (blue), 20% (green) and 30% (red). The pre-filtered signals are compared with simulated non-dispersive signals from the same numerical phantom. The MSE is below −100 dB for cases when the estimation error is less than 20%. However, the MSE is significantly high when the

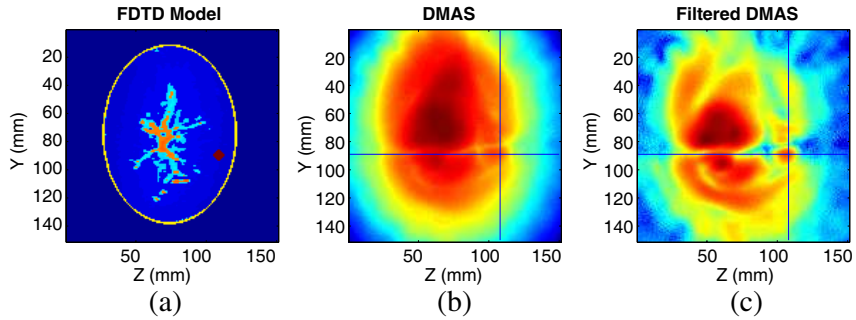

Figure 7. Effects of pre-filtering on the DMAS beamformer applied to a dense dielectrically-heterogeneous breast. While tumour detection is very difficult in such scenarios, the presence and location of the tumour only becomes discernible when pre-filtering is applied.

estimation error of average dielectric properties of the phantom is more than 20%. This reinforce the need to have an accurate average dielectric properties estimation algorithm.

The pre-filtering approach has been applied to Class 1 and Class 2 in the MRI-derived phantom repository. It is not clear if existing beamformers will successfully detect tumors in highly dense breast of Class 3 or Class 4. However, the study shows that the image created with pre-filtering method will be improved compared to any of the non-filtered beamformer used in this study. The method can be

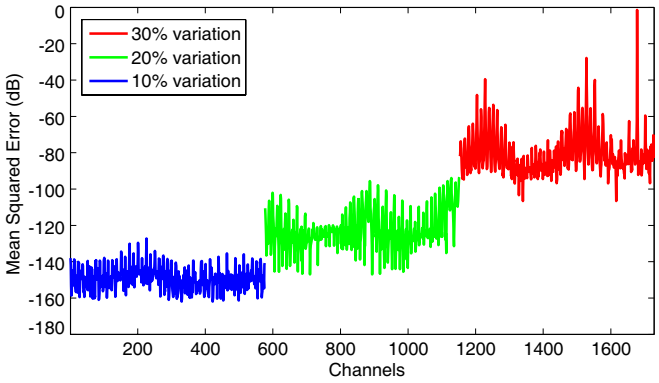

Figure 8. Effect of pre-filtering: Mean Squared Error (MSE) of filtered signals and simulated non-dispersive signals on three MRI-derived numerical breast models; BLUE) A model with less than 10% variation in average dielectric properties; GREEN) model with 20% variation; RED) model with 30% variation in average dielectric properties.

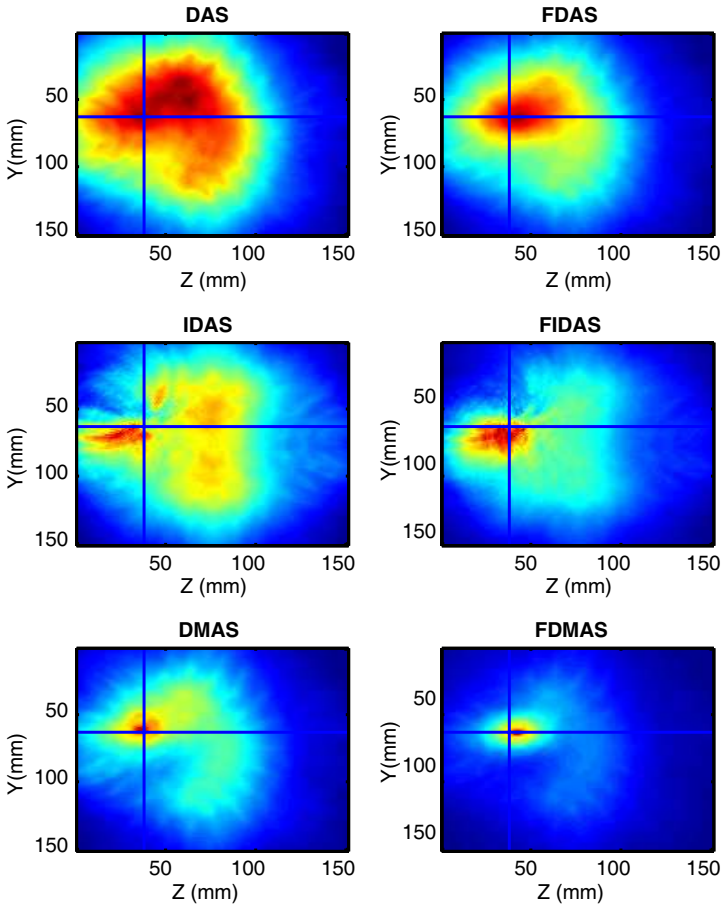

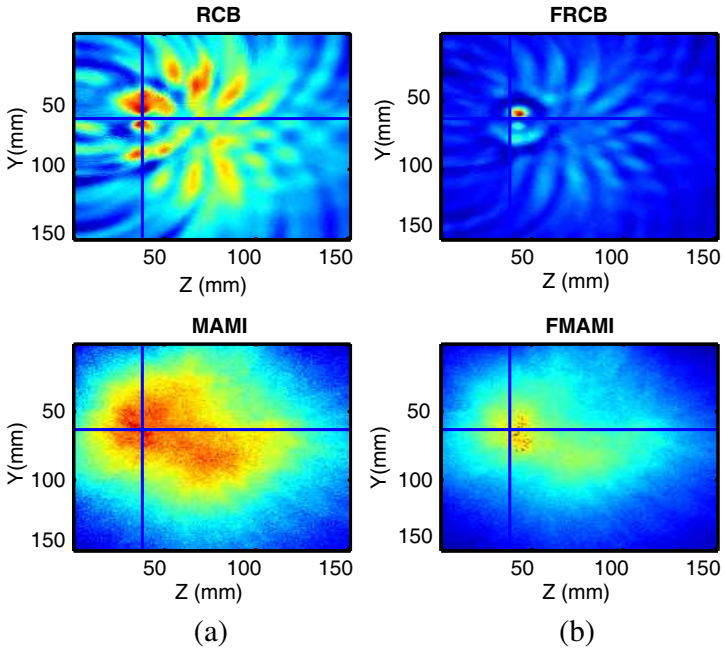

Figure 9. 2D slice of reconstructed energy maps with (b) pre-filtering and (a) without pre-filtering for all beamformers.

used in practical scenario if average dielectric properties can be estimated with less than 20% error and shape information is available to produce numerical model with minimal error.

6. CONCLUSIONS

A pre-filtering approach for CMI has been developed to compensate for dispersion introduced by normal breast tissue, across a range of data-dependent and data-independent beamforming algorithms, and over a range of potential clinical scenarios. It has been clearly shown that the proposed pre-filtering approach improves the performance of conventional beamformers, by compensating for attenuation and phase effects encountered by UWB signals as they propagate through the breast. This compensation, while not perfect due to intra-channel variations in dielectric properties, produces an improved breast image and enables enhanced detection of tumours located close to regions of fibro-glandular tissue compared to non-filtered beamformers. Moreover, the proposed method has shown improved clutter-suppression capabilities due to the normal heterogeneity of breast tissue. Future work will involve the study of the proposed preprocessing filter on experimental data where shape information will be obtained using a laser system such as [25].

ACKNOWLEDGMENT

This work is supported by Science Foundation Ireland (grant numbers 11/SIRG/I2120 and 12/IP/1523).

REFERENCES

1. American Cancer Society, "Breast cancer facts and figures 2012," Tech. Rep., Atlanta, GA, 2012.
2. Cancer Research UK, "Cancerstats — breast cancer — uk," Tech. Rep., London, UK, 2009.
3. Nass, S. L., I. C. Henderson, and J. C. Lashof, *Mammography and Beyond: Developing Technologies for the Early Detection of Breast Cancer*, National Academy Press, 2001.

4. Bird, R. E., T. W. Wallace, and B. C. Yankaskas, "Analysis of cancers missed at screening mammograph," *Radiology*, Vol. 184, 613–617, 1992.
5. Chaudhary, S. S., R. K. Mishra, A. Swarup, and J. M. Thomas, "Dielectric properties of normal and malignant human breast tissue at radiowave and microwave frequencies," *Indian Journal of Biochemistry and Biophysics*, Vol. 21, 76–79, 1984.
6. Joines, W., Y. Zhang, C. Li, and R. L. Jirtle, "The measured electrical properties of normal and malignant human tissues from 50 to 900 MHz," *Med. Phys*, Vol. 21, 547–550, 1994.
7. Souvorov, A., A. E. Bulyshev, S. Y. Semenov, R. H. Svenson, and G. P. Tatis, "Two dimensional analysis of a microwave at antenna array for breast cancer tomography," *IEEE Trans. Microwave Theory Tech.*, Vol. 48, No. 8, 1413–1415, August 2000.
8. Craddock, I. J., R. Nilavalan, A. Preece, and R. Benjamin, "Ex-perimental investigation of real aperture synthetically organised radar for breast cancer detection," *IEEE AP-S International Symposium*, Vol. 1B, 179–182, Washington, DC, 2005.
9. Hagness, S. C., A. Taove, and J. E. Bridges, "Two-dimensional FDTD analysis of a pulsed microwave confocal system for breast cancer detection: Fixed focus and antenna array sensors," *IEEE Transactions on Biomedical Engineering*, Vol. 45, 1470–1479, 1998.
10. O'Halloran, M., M. Glavin, and E. Jones, "Channel-ranked beamformer for the early detection of breast cancer," *Progress In Electromagnetics Research*, Vol. 103, 153–168, 2010.
11. O'Halloran, M., E. Jones, and M. Glavin, "Quasi-multistatic mist beamforming for the early detection of breast cancer," *IEEE Transactions on Biomedical Engineering*, Vol. 57, No. 4, 830–840, 2010.
12. Lazebnik, M., D. Popovic, L. McCartney, C. B. Watkins, M. J. Lindstrom, J. Harter, S. Sewall, T. Ogilvie, A. Magliocco, T. M. Breslin, W. Temple, D. Mew, J. H. Booske, M. Okoniewski, and S. C. Hagness, "A large-scale study of the ultrawideband microwave dielectric properties of normal, benign and malignant breast tissues obtained from cancer surgeries," *Phys. Med. Biol.*, Vol. 52, 6093–6115, 2007.
13. O'Halloran, M., E. Jones, and M. Glavin, "Effects of fibroglandular distribution on data-independent beamformering algorithms," *Progress In Electromagnetic Research*, Vol. 97, 141–158, 2009.
14. Shahzad, A., M. O'Halloran, E. Jones, and M. Glavin, "Prefiltered beamforming for early-stage breast cancer detection," *IEEE Antennas and Wireless Propagation Letters*, Vol. 12, 500–503, 2013.
15. Elahi, M. A., M. Glavin, E. Jones, and M. O'Halloran, "Artifact removal algorithms for microwave imaging of the breast," *Progress In Electromagnetics Research*, Vol. 141, 185–200, 2013.
16. Bond, E. J., X. Li, S. C. Hagness, and B. D. Van Veen, "Microwave imaging via space-time beamforming for early detection of breast cancer," *IEEE Transactions on Antennas and Propagation*, Vol. 51, No. 8, 1690–1705, 2003.
17. Winters, D. W., E. J. Bond, and S. C. Hagness, "Estimation of the frequency-dependent average dielectric properties of breast tissue using a time-domain inverse scattering technique," *IEEE Transactions on Antennas and Propagation*, Vol. 54, No. 1, 3517–3528, 2006.
18. Sarafianou, M., I. Craddock, T. Henriksson, M. Klemm, D. Gibbins, A. Preece, J. Leendertz, and R. Benjamin, "Music processing for permittivity estimation in a delay-and-sum imaging system," *7th European Conference on Antennas and Propagation (EuCAP)*, 839–842, 2013.
19. Bourqui, J. and E. Fear, "Systems for ultra-wideband microwave sensing and imaging of biological tissues," *7th European Conference on Antennas and Propagation (EuCAP)*, 834–835, 2013.
20. Zastrow, E., S. K. Davis, M. Lazebnik, F. Kelcz, B. D. Van Veen, and S. Hagness, "Development of anatomically realistic numerical breast phantoms with accurate dielectric properties for modeling microwave interactions with the human breast," *IEEE Trans. Biomed. Eng.*, Vol. 55, No. 12, 2792–2800, December 2008.
21. Lazebnik, M., M. Okoniewski, J. H. Booske, and S. C. Hagness, "Highly accurate debye models for normal and malignant breast tissue dielectric properties at microwave frequencies," *IEEE Microwave and Wireless Components Letters*, Vol. 17, No. 12, 822–824, December 2007, fitting Debye to the Cole cole models.

22. Klemm, M., I. Craddock, J. Leendertz, A. Preece, and R. Benjamin, "Improved delay-and-sum beamforming algorithm for breast cancer detection," *International Journal of Antennas and Propagation*, Vol. 2008, 2008.
23. Lim, H. B., N. T. T. Nhung, E.-P. Li, and N. D. Thang, "Confocal microwave imaging for breast cancer detection: Delay-multiply-and-sum image reconstruction algorithm," *IEEE Transactions on Biomedical Engineering*, Vol. 55, No. 6, 1697–1704, 2008.
24. Xie, Y., B. Guo, J. Li, and P. Stoica, "Novel multistatic adaptive microwave imaging methods for early breast cancer detection," *EURASIP Journal on Applied Signal Processing*, Vol. 2006, 1–13, 2006.
25. Bourqui, J., J. M. Sill, and E. Fear, "A prototype system for measuring microwave frequency reflections from the breast," *International Journal of Biomedical Imaging*, Vol. 2012, 2012.